Received: 18 April 2022 | Revised: 6 July 2022 | Accepted: 8 July 2022

DOI: 10.1111/cas.15499

ORIGINAL ARTICLE

Cancer Science WILEY

Clinical significance and immune landscape of KIR2DL4 and the senescence-based signature in cutaneous melanoma

Rui Mao[1] | Zhengyun Ren[2] | Fan Yang[3] | Peng Yang[4] | Tongtong Zhang[2,5]

[1]Department of Dermatology, Xiangya Hospital, Central South University, Changsha, China

[2]The center of Gastrointestinal and Minimally Invasive Surgery, Department of General Surgery, The Third People's Hospital of Chengdu, College of Medicine, Southwest Jiaotong University, Chengdu, China

[3]Emergency Department, Peking University Third Hospital, Peking University School of Medicine, Beijing, China

[4]Department of Pathology, The Third People's Hospital of Chengdu, The Affiliated Hospital of Southwest Jiaotong University, The Second Chengdu Hospital Affiliated to Chongqing Medical University, Chengdu, China

[5]Medical Research Center, The Third People's Hospital of Chengdu, The Affiliated Hospital of Southwest Jiaotong University, The Second Chengdu Hospital Affiliated to Chongqing Medical University, Chengdu, China

Correspondence
Tongtong Zhang, Medical Research Center, The Center of Gastrointestinal and Minimally Invasive Surgery, The Third People's Hospital of Chengdu, Chengdu 610031, Sichuan Province, China.
Email: 163zttong@163.com

Funding information
This work was supported by a grant from the National Natural Science Foundation of China (81502075). The funder had no role in the study design and implementation

Abstract

Senescence is an effective barrier to tumor progression. Mutations that inhibit senescence and promote cell division are mandatory for the development of cancer. Therefore, it is particularly important to explore the differences between cutaneous melanoma (CM) patients with severe and mild degrees of senescence. We clustered all the patients with CM in the Cancer Genome Atlas (TCGA) database based on all the genes of the senescence pathway in the CellAge and MSigDB database. The prognosis, immunotherapy effect, tumor microenvironment score, NRAS mutation rate, expression of CD274, CTLA4, and PDCD1, and abundance of $CD8^+$ T and natural killer (NK) cell infiltration in the younger group of patients (YG) were higher than those in the older group (OG). Compared with the American Joint Committee on Cancer (AJCC) stage, the risk scoring system stratified the risk of CM patients and guided immunotherapy more accurately. The nomogram model, which combined the AJCC stage and risk score, greatly improved the ability and accuracy of prognosis prediction. As KIR2DL4 is the core molecule in the risk scoring system (RSS), knocking down the KIR2DL4 of human NK cells in vitro can inhibit the cytotoxicity of NK cells and can also inhibit the secretion of tumor necrosis factor-α and interferon-γ by NK cells. In contrast, upregulation of KIR2DL4 can activate the MEK/ERK signaling pathway, which is the activation pathway of NK cells. Our RSS and nomogram model can accurately stratify the risk of CM patients and effectively predict the effect of immunotherapy and prognosis in CM patients.

KEYWORDS
cutaneous melanoma, immunotherapy, KIR2DL4, prognosis, senescence-related genes

Abbreviations: AJCC, American Joint Committee on Cancer; CM, cutaneous melanoma; DMFS, distant metastasis free survival; DSS, disease special survival; KIR, Killer cell immunoglobulin-like receptor; OG, older group of patients; OS, overall survival; RSS, risk scoring system; SASP, senescence-associated secretory phenotype; TCGA, the Cancer Genome Atlas; TME, tumor microenvironment; YG, younger group of patients.

1 | INTRODUCTION

Cutaneous melanoma is a fatal skin cancer that originates from melanocytes, which produce melanin in the skin. Over the past few decades, its incidence among White people has increased dramatically, with 230,000 new cases per year worldwide (World Health Organization).[1] While early localized malignant melanoma of the skin can be cured by surgery, the prognosis of metastatic melanoma is very poor. Although some patients with metastatic melanoma may benefit a lot from immunotherapy, other patients either develop drug resistance or do not experience any treatment effect. These clinical challenges drive us to discover new drug targets and drugs that can benefit patients who are inherently resistant to targeted therapy and immunotherapy.

Aging plays an important role in the regulation of cancer cells. The carcinogenic transformation of normal cells can lead to aging and initially prevent their growth. However, malignant cells typically bypass this process through gene mutation or the epigenetic downregulation of tumor inhibition-related pathways, such as the p53–p21 and $p16^{ink4a}$–RB pathways.[2] The age-related accumulation of SASP cells can promote cancer progression by reprogramming the primary and metastatic microenvironment (including the premetastatic niche) over time to a state more prone to malignant cell growth.[3] Senescent cells are produced throughout life and play a beneficial role in various physiological and pathological processes. In addition, with increasing age, the continuous accumulation of aging cells also brings adverse consequences. These nonproliferating cells occupy a key cell niche and synthesize proinflammatory cytokines, leading to diseases and incidence rates related to aging.[4]

CM is a complex tumor, and a variety of environmental and genetic factors are needed to guide the acquisition of malignant characteristics.[5] Recently, the immunotherapy of CM has made exciting progress and ushered in a new era of CM treatment. Immunotherapy can cause an unprecedented sustained response in patients with advanced cancer compared with response to conventional chemotherapy. However, this response occurs only in a relatively small number of patients. The positive response of immunotherapy typically depends on the interaction between tumor cells and immune regulation in the tumor microenvironment (TME). Under these interactions, the TME plays an important role in inhibiting or enhancing the immune response. Understanding the interaction between immunotherapy and the TME is not only the key to analyzing the mechanism, but also to providing new methods to improve the efficacy of immunotherapy. Exploring different senescence patterns among CM patients and their inherent TME differences, mutation landscape, immunotherapy effect, and prognosis can provide new insights into the mechanism of occurrence and development of CM and clinical treatment.

KIR is a transmembrane glycoprotein expressed by NK cells and T-cell subsets. KIR protein is considered to play an important role in the regulation of the immune response. KIR2DL4, with two Ig domains and a long cytoplasmic tail 4, is a type of KIR, but its association with CM has not been studied. Previous studies have suggested that HLA-G is recognized by KIR2DL4 receptors on NK cells, and this leads to immune tolerance and immune escape. However, in the absence of HLA-G, KIR2DL4 interacts with IFN-γ to promote the secretion of more proinflammatory and angiogenic factors in NK cells.[6,7] Therefore, it is speculated that there is some type of factor in melanoma that interacts with KIR2DL4 to promote NK cells to release cytotoxic factors to kill tumor cells.

Here, using the SKCM data from TCGA, we systematically studied the different aging modes of CM patients, as well as the differences in somatic mutation, TME, immunotherapy, and prognosis between the two modes. In addition, to guide the clinical practice, we constructed an RSS and a prognostic nomogram to better predict the effect and prognosis of immunotherapy. Finally, using functional experiments in vitro, we explore the mechanism of the senescence-related molecule KIR2DL4 in inhibiting the development of CM.

2 | MATERIALS AND METHODS

2.1 | Data collection and preprocessing

In this study, TCGA (https://portal.gdc.cancer.gov/) database provided a TCGA-SKCM data set as a training cohort, containing the gene expression matrix of 459 CM samples and their corresponding clinical follow-up data. The GSE22153, GSE15605, GSE22154, GSE43955, GSE46517, GSE54467, and GSE65904 data sets were downloaded from the GEO (https://www.ncbi.nlm.nih.gov/gds/) database. As for GSE54467 and GSE15605, we downloaded $\log_2$-transformed and quantile normalization matrix data, whereas GSE22153, GSE46517, GSE22154, GSE46517, and GSE65904 data sets were converted and normalized by $\log_2$ after download. Usually, we used the median of the expression value as the expression of genes with multiple probes. The downloaded matrix was an mRNA expression profile in fragments per kilobase of transcript per million format. The samples used in this study had to meet the following criteria[1]: samples with nonzero probe expression accounted for 80% of all samples[2]; patients had accurate survival status and follow-up time.

The GSE65904 data set, containing information about DSS (210 patients) and DMFS (150 patients), was used as a test cohort. In addition, the GSE22153, GSE22154, GSE46517, and GSE54467 data sets, containing only the OS data (236 patients), were integrated into the validation cohort. While integrating the validation data set, we used the combat function of R package "sva" to remove the batch effect. Table S1 shows the basic data of the data sets included in this study.

CellAge[8] (https://genomics.senescence.info/cells/), which contains 279 aging-related genes, is a database of genes associated with cell senescence. The Molecular Signatures Database (MSigDB)[9,10] is a collection of annotated gene sets for use with GSEA software. The three aging gene sets (GOBP_AGING, GOBP_CELL_AGING, and GOBP_CELLULAR_SENESCENCE) were downloaded from the MSigDB database (http://www.gsea-msigdb.org/gsea/msigdb/index.jsp). These three aging-related gene sets contained nearly all

the genes that play an important role in aging involved in the existing aging research ($n = 304$). We combined two aging-related gene data sets (CellAge and MSigDB) to obtain 313 aging-related genes. We intersected these 313 genes with TCGA-SKCM dataset and all genes in the GEO data set involved in this study using an upset analysis, and we finally obtained 221 aging-related genes. The "Upset" analysis was performed by executing the "Upset" function in the "UpSetR" package, and the VENN circle was drawn using the "ggvenn" function in the "yyplot" package.

2.2 | Associations between the cluster and immunity

The immune score and stromal score of each CM patient in TCGA-SKCM cohort were calculated using the ESTIMATE[11] and Xcell (https://xcell.ucsf.edu/)[12] website, and the differences in the immune score and stromal score among the different groups were further analyzed using the Wilcoxon test.[13] The estimate score is the combination of the stromal score and the immune score. It is an index to evaluate the purity of a tumor.[11] Based on the matrix of TCGA-SKCM cohort, we calculated the abundance of immune cells by using CIBERSORT,[14] MCP Counter,[15] TIMER (http://timer.comp-genomics.org/),[16] EPIC, and Xcell software packages and excluded the samples with $p > 0.05$. Finally, the Mann–Whitney U-test was used to analyze the differences in the immune cell subtypes among the different groups.

2.3 | Tumor somatic mutation analysis

The tumor mutation load (TMB) has attracted much attention in immunotherapy. TMB and PD-L1 are two important biomarkers to predict the response to PD-1 antibody therapy. We used the waterfall function of the "maftools" package to show mutations in patients with high senescence and low-risk scores in TCGA-SKCM cohort. Missense, nonsense, uninterrupted, silence, and frameshift/in-frame insertions and deletions were counted, while synonymous mutations were excluded.[17] The total number of somatic mutations was used to calculate the TMB score. According to the median of the TMB score, all CM samples with somatic mutations in TCGA data set were divided into a high TMB score group and a low TMB score group.

2.4 | Prognostic assessment using the RSS

By using the "Survival" package of R software, we used a univariate Cox analysis to calculate the prognostic value of each SRG and selected an SRG as the seed SRG for the Cox-lasso regression analysis. Then, a multivariate Cox regression analysis was performed to evaluate the prognostic characteristics of each SRG using the R packages "Survminer", "Glment", and "Survival". The risk score of each patient in the training group was calculated using the Cox proportional hazards model (PH model): $\hat{h}_i(t) = \hat{h}_0(t)\exp\left(x_i'\hat{\beta}\right)$ (where exp is the prognostic gene expression level; β is the multivariate Cox regression model regression coefficient; and $h_0(t)$ is the baseline hazard function. This is a function that describes the "instantaneous mortality" that specifically refers to the instantaneous mortality of the observed object at the time of survival to t). All of the CM samples were randomly divided into a high-risk score group and a low-risk score group according to the median of the risk score. The Kaplan–Meier method was used for the survival analysis, and the log-rank test was used to compare survival between the groups. The R software package, "SurvivalROC", was used to draw the receiver operating characteristic curve (ROC) curve and calculate the corresponding area under the curve (AUC).

3 | RESULTS

3.1 | Cluster 1 showed great advantages in survival and nonrecurrence compared with cluster 2

Figure S1 shows the entire analytical process of the study.

First, we screened the coexisting SRGs in TCGA, GSE22153, GSE22154, GSE46517, GSE54467, and GSE65904 databases using UPSET and identified a total of 221 SRGs (Figure S2A). Then, we merged four data sets, GSE22153, GSE22154, GSE46517, and GSE54467, and eliminated the batch effect (Figure S2B). The results of the principal component analysis (PCA) before and after merging the data sets showed that the batch effect was well eliminated (Figure S2C,D). The determination of the K value is very important for the consistency of a cluster analysis. When the cumulative distribution function (CDF) reaches the approximate maximum value, the cluster analysis result is the most reliable. Typically, a K value with small decline slope of the CDF is used. Based on unsupervised clustering, TCGA-SKCM was divided into two clusters (Figure 1A,B). According to this method, it is really the best when $k = 2$. According to the results of prognostic analysis between the two groups, cluster 1 showed great advantages in survival and nonrecurrence (Figure 1C,D). Figure 1E shows a multivariate heat map that contains data on the expression of 221 SRGs and clinicopathological data. There was a significant difference in the multiple SRGs between the two clusters (Figure 1F). The age of patients in cluster 2 was significantly higher than that of patients in cluster 1 (Figure S3A). Therefore, we labeled the clusters 1 and 2 as the younger group (YG) and older group (OG), respectively.

3.2 | YG was primarily enriched in the immune response and immunotherapy pathways

We analyzed the differential expression of 58,385 probes between the YG and OG and found that 356 protein-coding genes were

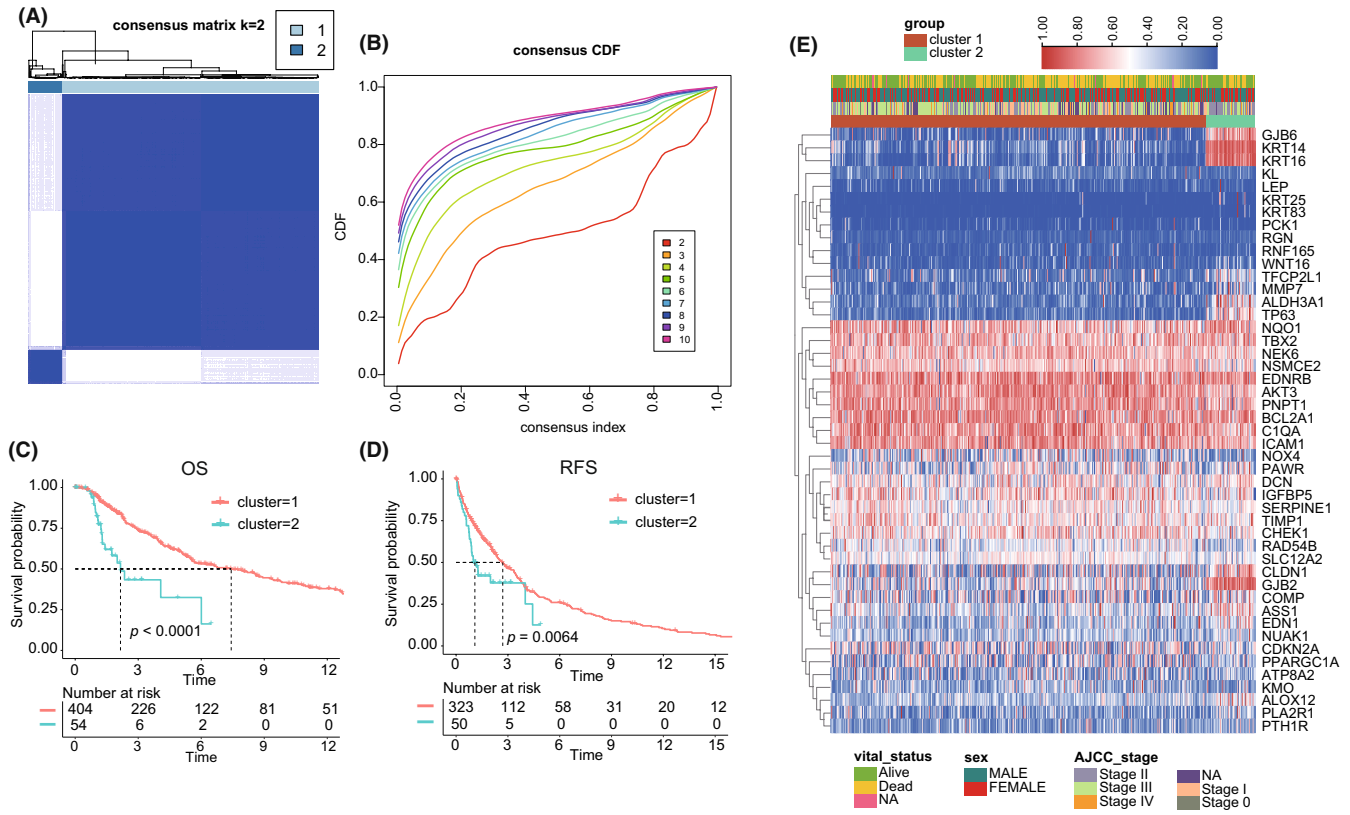

FIGURE 1 Unsupervised clustering for SRGs. (A, B) Classification of TCGA-SKCM into two groups. When the cumulative distribution function (CDF) reaches the approximate maximum value, the cluster analysis result is the most reliable. Typically, a K value with a small decline in the slope of the CDF is used. (C, D) Kaplan–Meier curves of OS and RFS in the training cohort based on clustering. (E) Landscape of the expression of significantly differentially expressed SRGs in TCGA-SKCM cohort

upregulated in the OG, and 1048 protein-coding genes were upregulated in the YG (Figure S3B). The upregulated genes in the OG and YG were analyzed using a functional enrichment analysis of the Gene Ontology Biological Processes (GO-BP) and Kyoto Encyclopedia of Genes and Genomes (KEGG) pathways, respectively. The results of the KEGG and GO-BP analyses showed that the upregulated genes in the YG were primarily concentrated in the T-cell-receptor signaling pathway, the B-cell-receptor signaling pathway, the positive regulation of lymphocyte activation, the positive regulation of biological process, PD-L1 expression, and the PD-1 checkpoint pathway in cancer, and Th17 cell differentiation (Figure 2A,B). According to the KEGG and GO-BP analysis, the upregulated genes in the OG were primarily concentrated in the skin epidermis development, the regulation of epidermis development, the regulation of epidermal cell differentiation, the IL-17 signaling pathway, the extracellular matrix (ECM)–receptor interaction, skin development, and the adaptive immune response (Figure 2C,D). The upregulated genes in the YG were primarily enriched in the immune response and immunotherapy pathways, whereas those in the OG were primarily enriched in the aging-related pathways, such as cell and epidermal development and differentiation. Therefore, we speculated that the immune landscape and response to immunotherapy between the YG and the OG may be different.

3.3 | Difference in the immunotherapy response and immune landscape between the OG and the YG

Based on the results of the TIDE analysis, we further found that the response of patients in the YG to the immune checkpoint blockade was significantly higher than that in the OG (Figure 3A,B). In addition, the Kaplan–Meier (KM) analysis in patients who received immunotherapy and chemotherapy showed that the response of patients in the YG to immunotherapy and chemotherapy was significantly better than that of patients in the OG (Figure 3C,D). In addition, we compared the expression of multiple immune checkpoints in the B7 family and the CD28 family between the YG and the OG. The results showed that the expression levels of CD274, CTLA4, PDCD1, CD80, CD86, CD28, ICOS, and ICOSLG in the YG were significantly higher than that in the OG (Figure 3E). To explore the mechanism between the immunotherapy response and the tumor immune microenvironment, we further evaluated the differences in the tumor immune microenvironment between the two groups. The TME contains immune, interstitial, and endothelial cells, as well as inflammatory mediators and ECM molecules.[13] The results showed that the immune, stromal, and estimated scores of patients in the YG were significantly higher than those of patients in the OG (Figure S4A). The results of

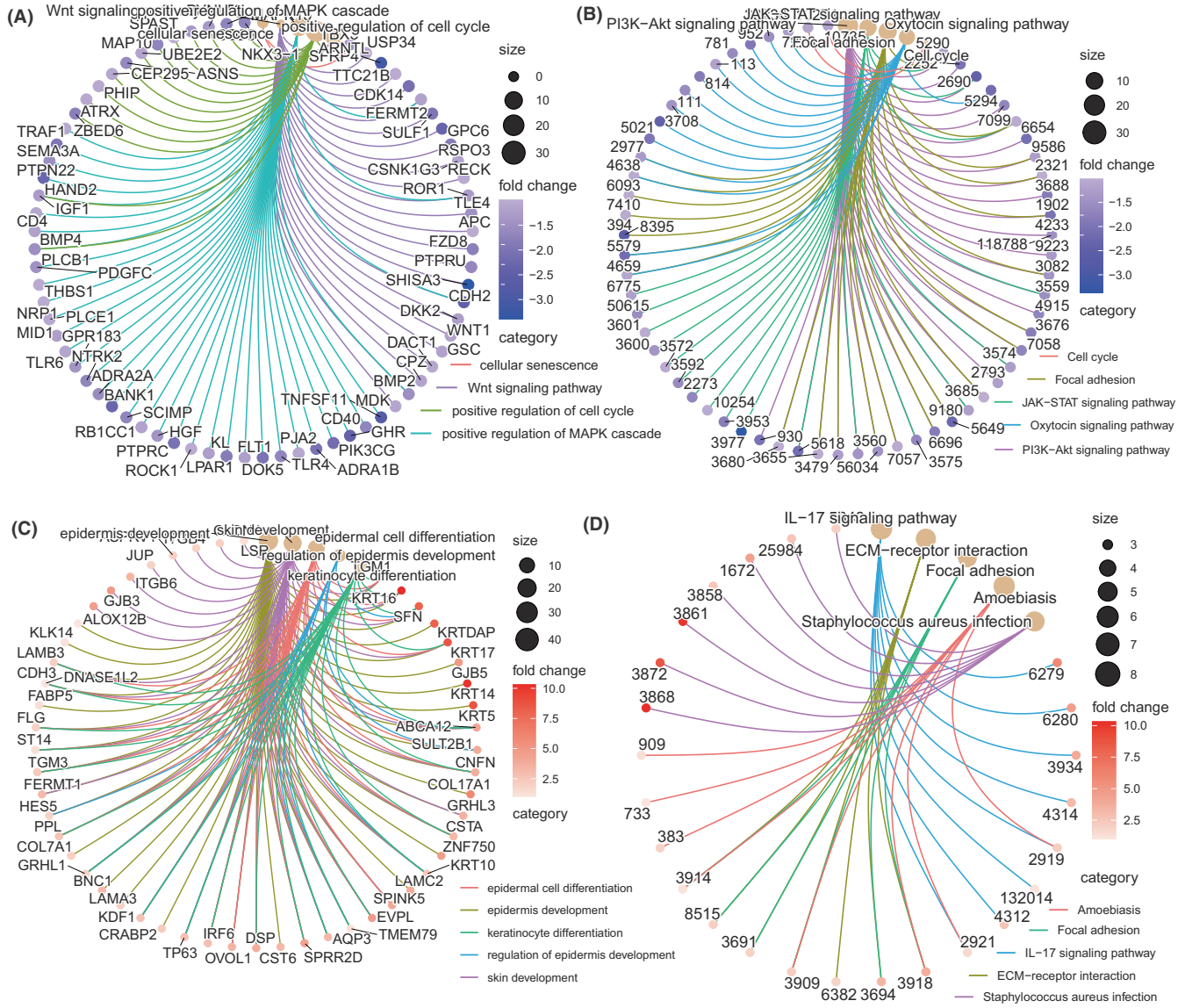

FIGURE 2 Enrichment analysis of differentially expressed genes between the YG and the OG. (A, B) Results of KEGG and GO-BP analysis of upregulated genes in the YG. (C, D) Results of the KEGG and GO-BP analyses of the upregulated genes in the OG

Xcell validated that the tumor immune microenvironment score of the YG was higher than that of the OG (Figure S5C). Through a KM analysis, we found that the prognoses of CM patients with higher stromal scores, immune scores, and ESTIMATE scores were better than that of CM patients with lower scores (Figure S4B–D).

Based on the fact that the prognosis of patients with different immune scores was quite different, we further explored the landscape of immune infiltration between the two groups of patients. Through a comparative analysis of the results of CIBERSORT and MCPcounter, we found that the infiltration abundances of $CD8^+$ T cells, NK cells, monocyte lines, macrophage cell line, and B-cell lines in patients in the YG were significantly higher than that in patients in the OG, while the abundances of neutrophils in the YG was significantly lower than that in patients in the OG (Figure S6A,B,D). Then, by regarding immune cells as prognostic factors and combining them with prognostic data, a univariate Cox regression analysis was conducted for each type of immune cells. We found that the $CD8^+$ T cells, NK cell lines, B-cell lines, monocyte lines, and macrophage cell line were associated with a better prognosis in patients with CM (Figure S6C,E). In addition, we compared the results of TIMER, EPIC, and Xcell and found that the $CD8^+$ T cells, NK cells, monocyte lines, and B-cell lines in patients in the YG were still significantly more abundant than those in patients in the OG (Figure S5A–C). Moreover, the abundance of melanocyte infiltration in patients in the OG was higher than that in patients in the YG (Figure S5C). The univariate Cox analysis also revealed that the abundances of B cells, NK cells, $CD8^+$ T cells, B-cell lines, and dendritic cells were associated with a better prognosis in patients with CM (Figure S7A–C). The abundance of melanocytes was associated with a poor prognosis in patients with CM (Figure S7A).

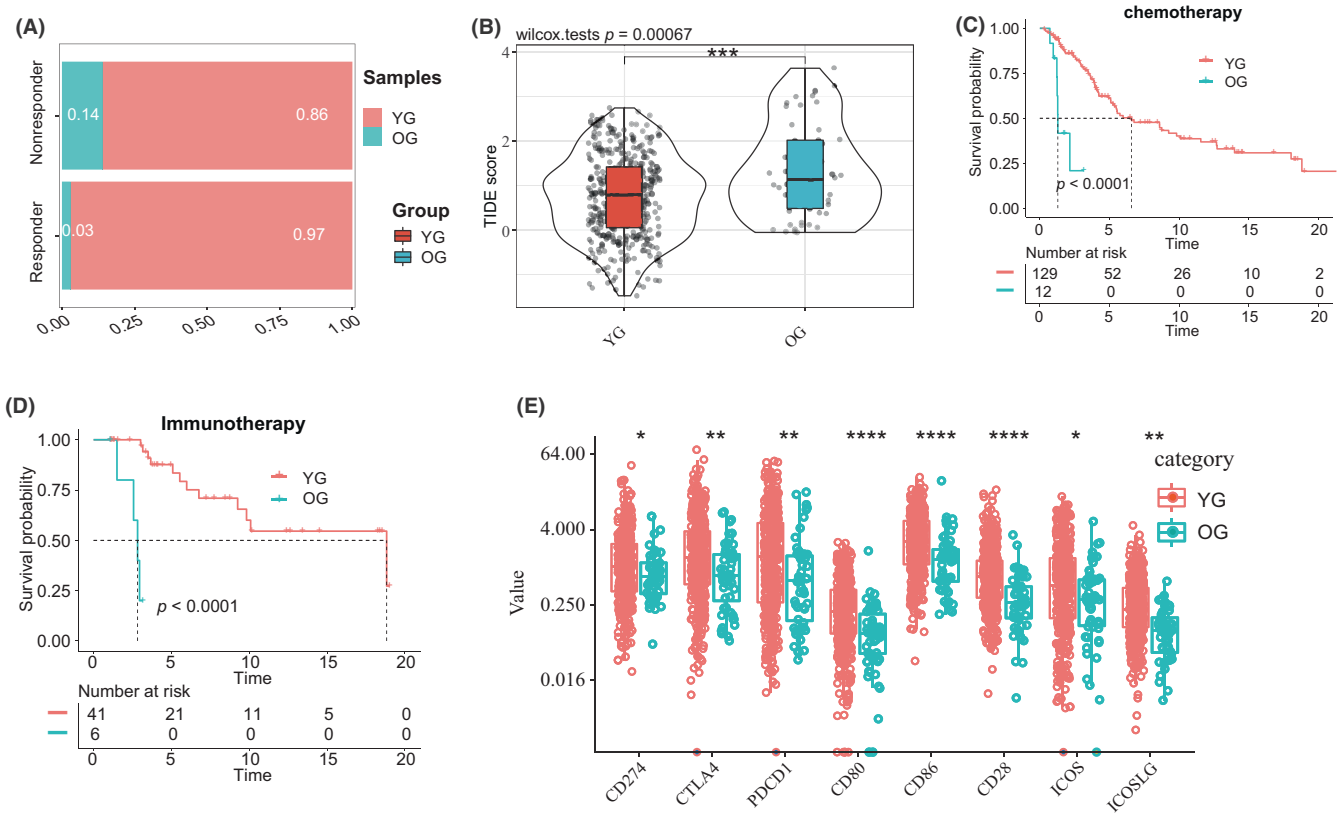

FIGURE 3 Difference of immunotherapy response and immune landscape between the OG and the YG. (A, B) Based on the results of TIDE analysis, we compared the efficacy of immune checkpoint blockade and TIDE score in patients in the OG and the YG. (C, D) The KM analysis of patients in the two clusters who had received immunotherapy and chemotherapy. (E) Differential expression of common immune checkpoint molecules between the YG and the OG

3.4 | The TMB of the YG was significantly higher than that of the OG

Figure S8 shows a summary of mutations in the CM patients in TCGA database provided by "maftool". The mutation waterfall map (Figure S9) of all the CM patients indicates that the mutation rate of BRAF in CM patients was 47%. The mutation rate of recorder NRAS was 25%. Through the somatic mutation analyses of the YG and the OG, we showed that the total mutation rate and the mutation rate of common mutation genes in the OG were lower than those in the YG (Figure S10A,B). By calculating the tumor mutation load scores of the two groups, we found that the TMB of the YG was significantly higher than that of the OG (Figure S10D). The KM analysis showed that the prognosis of the CM patients with high TMB scores was significantly better than that of the CM patients with low TMB scores (Figure S10C). In addition, the NRAS mutation rate (21%) in the YG was significantly lower than that in the OG (38%) (Figure S10E).

3.5 | Construction of the RSS for CM

In total, 94 SRGs ($p < 0.05$) selected using the univariate Cox regression analysis were included in the LASSO regression analysis (Figure S11A). According to the standard of lambda.1se (lambda value = 4) (Figure S11B,C), four molecules, namely, IL15, B2M, FOXM1, and KIR2DL4, were selected for the multivariate Cox regression analysis (Figure S11D). We calculated the risk score of the RSS according to the formula and according to the median risk score, and the CM patients in the training cohort and validation cohort were divided into a high-risk score group and a low-risk score group (Figure S12A,B). We found a significant difference in the expression of the four SRGs between the high-risk score group and the low-risk score group in both the training cohort and the validation cohort (Figure S12C,D). It was obvious that the expression of KIR2DL4 in the low-risk score group was significantly higher than that in the high-risk score group. In contrast, the expression of FOXM1 in the low-risk score group was significantly lower than that in the high-risk score group.

To validate the prognostic ability of RSS, we performed ROC and KM analyses. In the training and validation cohorts, the OS and recurrence free survival (RFS) of the low-risk score group were significantly better than those of the high-risk score group (log-rank test p-value < 0.0001, Figure S13A,C,D). The results of the ROC analysis showed that the AUC of 5-year OS in the training and validation cohorts was 0.711 and 0.830, respectively (Figure S13B,E). To further understand whether RSS has the same predictive effect on DSS and DMFS in patients with CM, we performed a similar

analysis in the test cohort ($n = 210$). Similarly, the DSS and DMFS of CM patients with high-risk scores were significantly lower than those of CM patients with low-risk scores (log-rank test p-value <0.001; Figure S13F,H). In addition, the ROC analysis showed that the RSS predicted that the AUC of 3-year DSS and DMFS in patients with CM was 0.661 and 0.698, respectively (Figure S13G,I). These results suggest that RSS can accurately predict the prognosis of patients with CM.

Based on the results of the TIDE analysis, we further found that the response to the immune checkpoint blockade among patients in the high-risk score group was significantly lower than that in the low-risk score group (Figure 4B,C). In addition, the KM analysis of the two groups of patients who received immunotherapy and chemotherapy showed that the response of the low-risk score group to immunotherapy and chemotherapy was significantly better than that of the high-risk score group (Figure 4A,D). In addition, we compared the expression differences of multiple immune checkpoints in the B7 family and CD28 family between the low-risk score and high-risk score groups. We found that the expression levels of CD274, CTLA4, PDCD1, CD80, CD86, CD28, ICOS, and ICOSLG in the low-risk score group were significantly higher than those in the high-risk score group (Figure 4E).

3.6 | Difference in the expression of four molecules in the RSS between CM and normal skin tissues

Based on the results of GEPIA2, the expression levels of B2M, KIR2DL4, and FOXM1 in CM patients were significantly higher than those in normal skin tissues, but there was no significant difference in the expression of IL15 between the two groups (Figure 5A). Next, we verified the expression of these four genes in two CM cohorts containing normal skin tissue samples. The results showed that the expression levels of B2M, FOXM1, and KIR2DL4 were still high in CM patients. Surprisingly, in the GSE46517 cohort, the expression of IL15 in the tumor group was significantly higher than that in the normal skin tissue (Figure 5B,C).

3.7 | Validation of the RSS in various clinical subgroups

Clinically, the pathological stage[18] is an important factor that affects the survival of patients with CM, whereas other key factors include sex and age.[19] Therefore, we validated the ability of RSS to predict

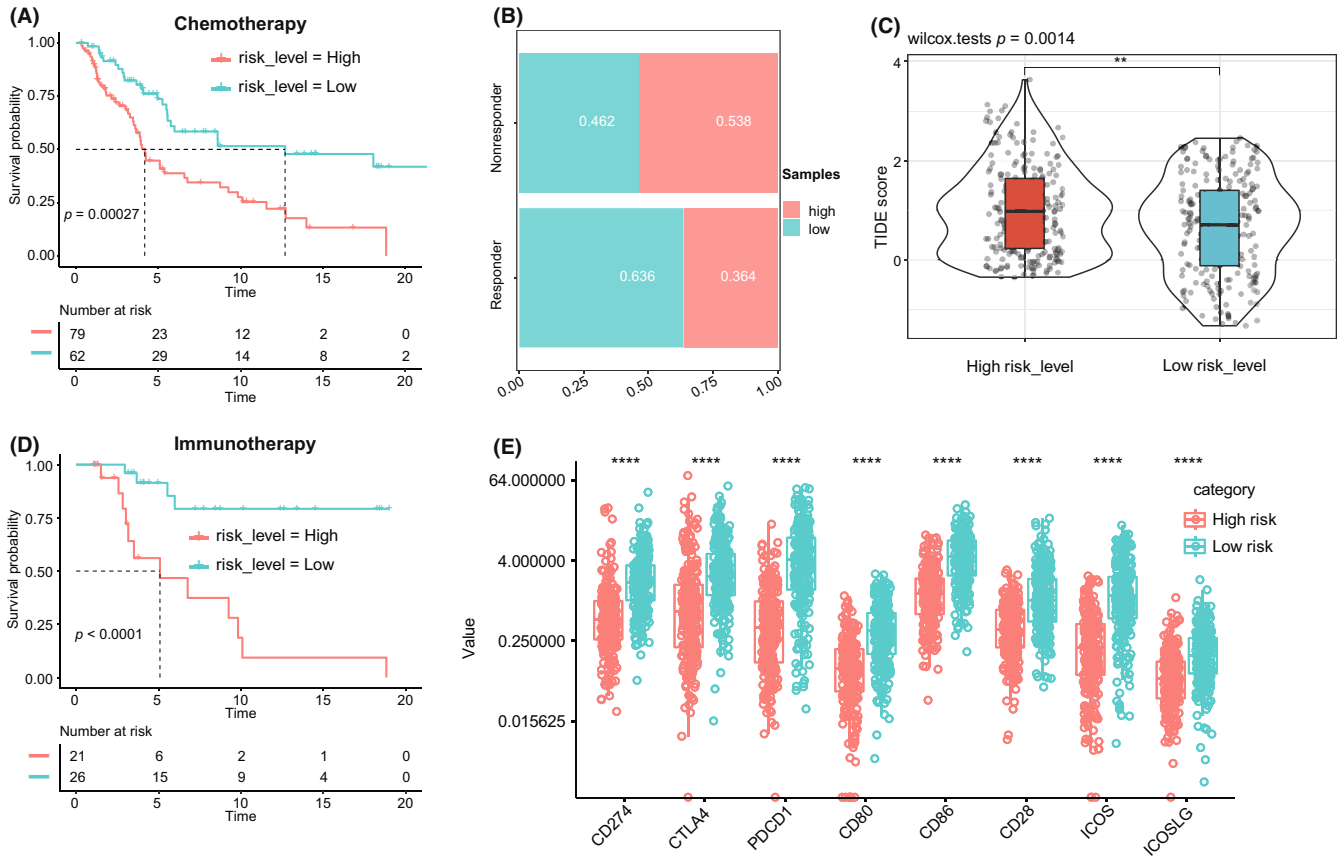

FIGURE 4 Difference in the immunotherapy response between the high-risk and low-risk score groups. (A, B) Based on the results of the TIDE analysis, we compared the efficacy of the immune checkpoint block and the TIDE score in patients of the high-risk and low-risk score groups. (C) Differential expression of common immune checkpoints between the high- and low-risk score groups. (D, E) KM analysis of the patients who had received immunotherapy and chemotherapy between the high-risk and low-risk score groups

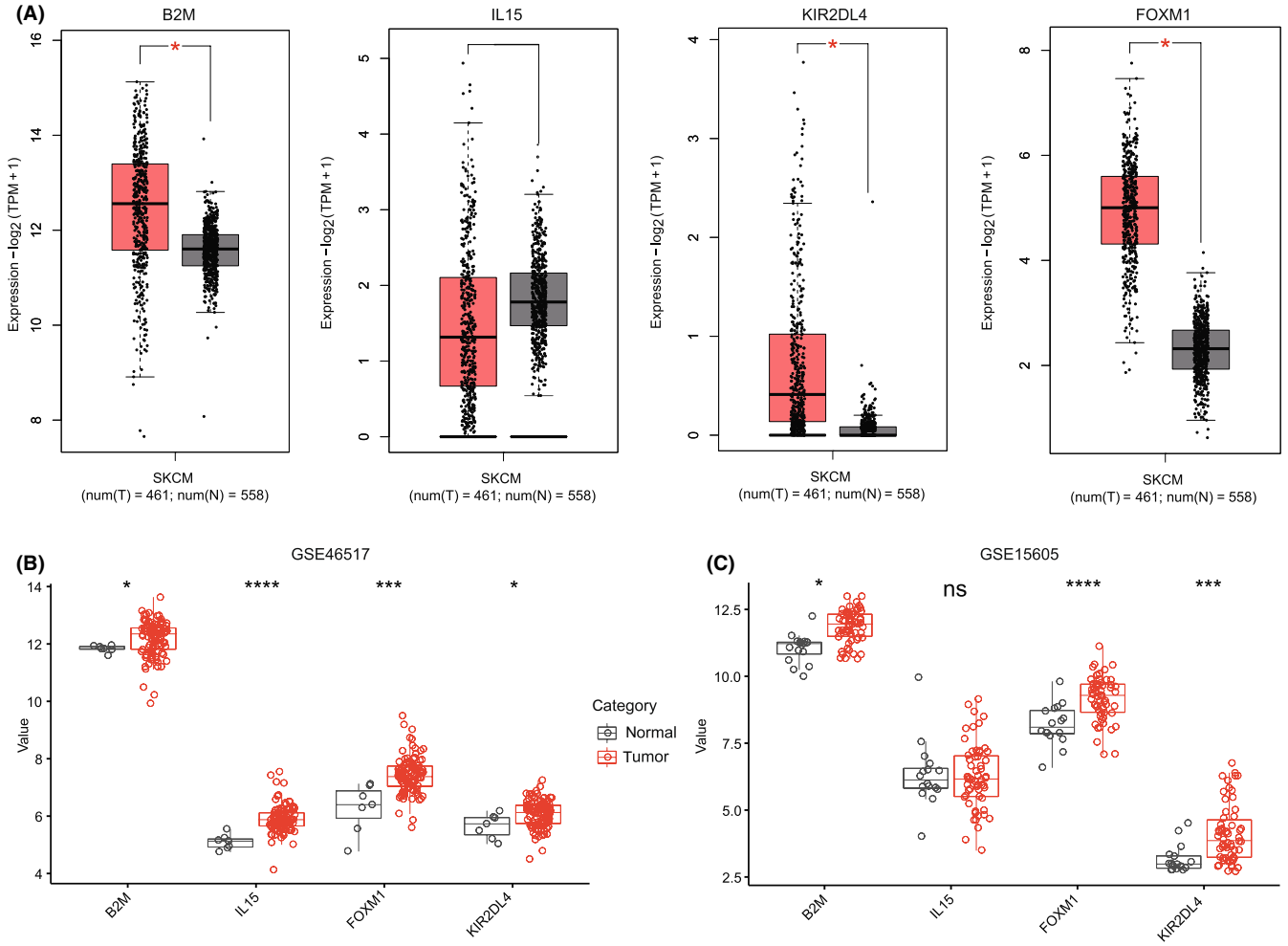

FIGURE 5 The difference in the expression of RSS molecules between CM tissues and normal skin tissues. (A) Difference in the expression of RSS molecules between CM tissues in TCGA and normal skin tissues in GTEx. (B, C) Difference in the expression of RSS molecules between CM tissues and normal skin tissues in GSE15605 (C) and GSE46517 (B). Red represents tumor tissue; gray represents normal tissue

the prognosis of CM patients in different stages, age, and sex, both in the training and the validation cohorts. RSS accurately stratified the risk in all four stages, both sexes, and both age categories (age ≥ 65 years and age < 65 years) (Figure S14).

3.8 | KIR2DL4 activated NK cells by activating the MEK/ERK pathway

We obtained 13 frozen samples of skin melanoma patients who received nivolumab (NIVO) (PD-1 inhibitors) and ipilimumab (IPI) (CTLA-4 inhibitors) treatment from March 2018 to March 2022 from the Department of Pathology of the third people's Hospital of Chengdu. The methodology of immunohistochemistry and immunofluorescence had been provided in the supplementary document of the manuscript. Immunohistochemical and immunofluorescence staining were performed on it (Figure S15A,B). Obviously, the results of immunofluorescence suggest that KIR2DL4 is indeed co-located with NK cells. The results from immunohistochemistry showed that, among the 13 specimens, 7 had high expression of KIR2DL4 and 6 had low expression. The OS time of CM patients with high expression of KIR2DL4 was significantly longer than that of patients with low expression of KIR2DL4 in CM patients (Figure S15C). In addition, the results of Kaplan–Meier analysis also suggested that OS in patients with high expression of KIR2DL4 was better than that of patients with low expression of KIR2DL4 (Figure S15D).

We isolated NK cells from melanoma tissue using flow cytometry (Figure S15A) (sorting–culture–re-sorting–re-nourishment). We first explored whether KIR2DL4 directly regulated the cytolytic activity of NK cells. We knocked down KIR2DL4 from the isolated NK cells with siRNA, and then we washed and co-cultured with melanoma cells to evaluate the cell lytic activity using a lactate dehydrogenase (LDH) assay. As shown in Figure S15B, the cytolytic activity of the NK cells decreased significantly compared with the control group, and the maximum killing rate was 1/4 of that of the control group. Next, we used enzyme-linked immunosorbent assay (ELISA) to evaluate the effect of KIR2DL4 on the cytokine production in the NK cells. As shown in Figure S15C,D, the KIR2DL4

knockdown significantly reduced the production of IFN-γ and TNF-α by the NK cells. To explore how KIR2DL4 activates NK cells, we constructed an overexpression plasmid of KIR2DL4 and transfected it into the NK cells. The results showed that the classical NK cell activation pathway, namely, the MEK/ERK signal pathway, was significantly activated, and the phosphorylated MEK/ERK protein was significantly upregulated after overexpression of KIR2DL4 (Figure S15E).

3.9 | Establishment of a nomogram based on the RSS and clinical features

To further stratify the risk in CM patients and validate the prognostic predictive ability of RSS, we constructed a prognostic nomogram. We included four variables, including age, sex, stage, and the risk score, into univariate and multivariate Cox regression analyses (Figure 6A,B). The risk score was independently associated with poor prognosis of patients with CM (HR = 2.613, $p < 0.05$). Next, we used these four features to construct a prognostic nomogram, and each subtype of the clinical features in this model corresponded to a specific score (Figure 6C). The vertical red line in the figure indicates the score of a CM patient (TCGA-DA-A960-01) included in the model. She was female, 73 years old, the AJCC grade was grade II, and the risk score was 1.711751, belonging to the high-risk score group. After calculation, her total risk score was 180, and the probability that her survival time was less than 3 years, 5 years, and 7 years was 0.517, 0.694, and 0.832 respectively. In fact, her survival time was 804 days, less than 3 years. The above results verified that our prognosis prediction model was accurate and effective. Finally, the total score of all clinical factors corresponded to a specific 3-, 5-, and 7-year survival probability. The C index of the nomograms of the training cohort and the validation cohort were 0.697 (95% CI, 0.695–0.699) and 0.762 (95% CI, 0.746–0.778), respectively. The calibration curve of the training cohort showed that the predicted values were consistent with the observed values of the 3-, 5-, and 7-year OS (Figure 6E). We calculated the total risk score of each patient according to each predictor in the nomogram model and took the median total risk score as the cut-off value to divide all CM patients into high-risk patients and low-risk patients. The KM analysis showed that the survival of high-risk patients was significantly poorer than that of low-risk patients (Figure 6D). The ROC analysis showed that the AUC values of 3-year, 5-year, and 7-year prognosis of CM patients by the total risk score reached 0.767, 0.758, and 0.781, respectively (Figure 6G). In addition, the AUC value of the total risk score was always higher than that of the AJCC stage. Finally, the clinical decision curve analysis showed that the patient benefit rate of the model excluding the risk score was significantly lower than that of the model excluding the AJCC stage (Figure 6F). Unsurprisingly, the model that included both the risk score and the AJCC stage showed the highest clinical benefit rate. In addition, The validation cohort can accurately validated the model (Figure S17).

3.10 | GSEA

The results of GSEA showed that the cell cycle pathway was enriched in the high-risk score group (Figure S18). However, the pathways that were enriched in the low-risk score group were mainly the immune response-related pathways, such as the T-cell-receptor signaling pathway, B-cell-receptor signaling pathway, NK cell-mediated cytotoxicity, primary immunodeficiency, cell adhesion molecules (CAM), cytokine–cytokine receptor interaction, NOD-like receptor signaling pathway, PD-L1 expression, and the PD-1 checkpoint pathway in cancer, JAK/STAT signaling pathway, and Toll-like receptor signaling pathway. This suggested that the patients in our low-risk score group were in a state of immune activation, and the effect of immunotherapy was better.

4 | DISCUSSION

Aging skin promotes the metastasis of CM because when fibroblasts are aging, ECM components are more single, and collagen cross-linking and ECM contractility are reduced, and this inhibits the migration and recruitment of immune cells.[20] The aggregation of $CD4^+$ T cells and $CD8^+$ T cells increases the immune ability and antitumor activity in CM.[21,22] NK cells are cytotoxic innate lymphocytes, which can produce effective responses to a variety of tumor cells.[23] NK cells contribute to the editing of cancer immunity and are often defective or dysfunctional in cancer patients. The decrease in the number of NK cells and $CD8^+$ T cells is associated with adverse outcomes.[24] Tumor-induced neutrophils acquire the ability to inhibit cytotoxic T lymphocytes carrying CD8 antigen, which limits the metastasis of CD8 T cells,[25] affecting immunotherapy and this is not always conducive to the prognosis.[26]

In this study, we used the senescence gene set to divide CM patients into the YG and the OG. The immune score, stromal score, and TME score of the YG were higher than those of the OG. In addition, the results from five types of software for estimating the abundance of immune cell infiltration in tumor tissues showed that the abundance of B-cell line, $CD4^+$ T cells, $CD8^+$ T cells, NK cells, monocytes, and macrophages in patients in the YG was higher than that in patients in the OG. However, the neutrophils in the YG were significantly lower than those in the OG. Univariate Cox regression analysis showed that $CD8^+$ T cells, $CD4^+$ T cells, and NK cells were protective factors for the prognosis of CM patients. Therefore, we speculated that the prognosis and response to immunotherapy in the YG were better than those in the OG. The subsequent TIDE and KM analyses confirmed our assumption. The possible mechanism is that the abundance of targeted cells such as $CD8^+$ T cells and NK cells in the tumor tissues of patients in the YG is higher than that in the OG and that the expression of immune checkpoint molecules such as PD-L1 and CTLA4 is higher than that in the OG, which can improve the effect of immunotherapy and prognosis.

TMB has attracted much attention in immunotherapy. TMB and PD-L1 are two important biomarkers to predict the therapeutic

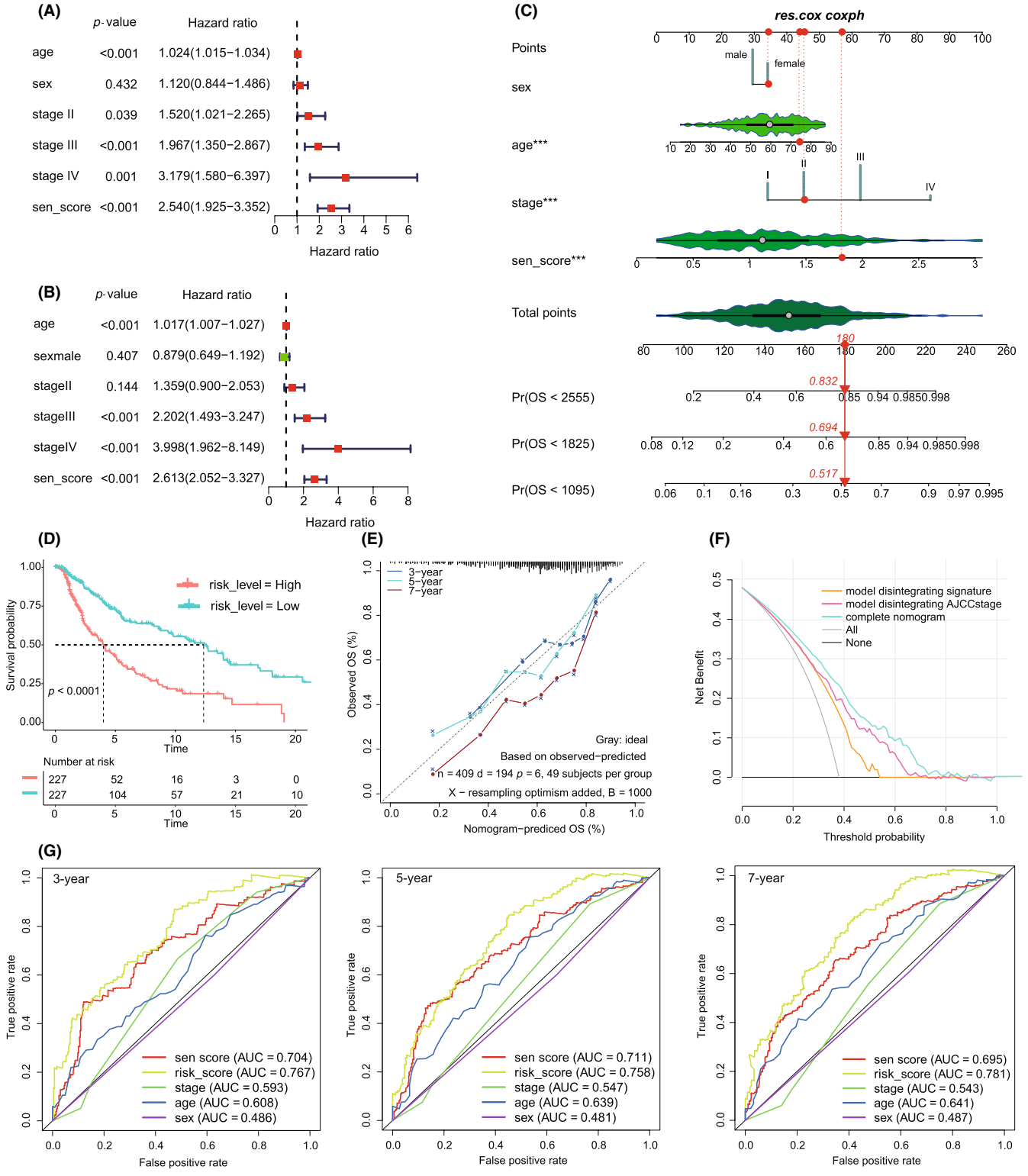

FIGURE 6 Construction and validation of the prognostic nomogram. (A, B) The univariate and multivariate Cox regression model. (C) The nomogram model was built by using the coefficients of the multivariate Cox regression model. (D) The Kaplan–Meier analysis showed that patients with a high-risk score had an obviously poor OS than patients with a low-risk score. (E) According to the calibration curve, predictive values were consistent with observed values, considering the probabilities of 3-year, 5-year, and 7-year OS. (G) The AUC values for 3-, 5-, and 7-year survival using the predictive nomogram reached 0.767, 0.758, and 0.781, respectively. (F) Finally, clinical decision analysis (DCA) showed that the clinical benefit rate of the model without AJCC stage alone was higher than that of the model without RSS

effect of PD-1 antibody.[27] According to Hodi et al.,[28] in patients who received an anti-PD-1 inhibitor NIVO or NIVO combined with anti-CTLA-4 inhibitor IPI or IPI alone, high (>median) TMB was associated with longer survival than low (≤median) TMB. In our study, the TMB score of the YG was significantly higher than that of the OG, and the prognosis of CM patients with a high TMB score was significantly better than that of patients with a low TMB score. The NRAS mutation is one of the mutation subtypes in patients with CM, which occurs in ~25% of patients. NRAS-mutant melanoma is more invasive, resulting in a lower median OS time and lagging treatment options.[29-31] Our results showed that the NRAS mutation rate of the OG was higher than that of the YG, but the specific mechanism needs to be further explored. In addition, the upregulated genes in the YG were mainly enriched in the immune response and immunotherapy pathways, while those in the OG were mainly enriched in aging-related pathways such as cell and epidermal development and differentiation. Therefore, we speculate that patients in the YG have higher immune activity and better response to immunotherapy, while patients in the OG age more severely.

Although the recent use of targeted therapy (BRAF, MEK) and immunotherapy (anti-CTLA-4, anti-PD-1) has significantly prolonged the median OS of patients with metastatic melanoma,[32] the treatment is far from perfect because the clinical response is either short-lived or restricted to a limited subgroup of melanoma patients.[33] Therefore, developing biomarkers that can predict the effect of immunotherapy would provide a more accurate treatment plan for patients with CM. We found that the survival time, status, and recurrence survival rate of CM patients in the YG were significantly higher than those of patients in the OG. The upregulated genes in the YG were mainly enriched in immune response and immunotherapy pathways, whereas those in the OG were mainly enriched in senescence-related pathways such as cell and epidermal development and differentiation. In addition, we also found that the effect of chemotherapy and immunotherapy and the response rate to immunotherapy in the YG were higher than those in the OG. Therefore, we speculate that senescence may affect the survival of patients with CM and the effect of immunotherapy.

To further develop more practical and convenient senescence-related biomarkers for predicting prognosis and immunotherapy effect, we screened out four SRGs that independently affected the prognosis of patients with CM and constructed a set of risk scores based on them. The KM and ROC analyses suggested that the RSS was able to accurately stratify the risk of CM patients and effectively predict the OS, RFS, DSS, and DMFS of CM patients. Surprisingly, the effect of chemotherapy and immunotherapy and the overall prognosis of patients with high aging score were significantly poorer than those of CM patients with low aging score. The expression of CD274, CTLA4, PDCD1, CD80, CD86, CD28, ICOS, and ICOSLG in the low-risk score group was significantly higher than that in the high-risk score group. Therefore, RSS can accurately predict the prognosis and immunotherapy effect of patients with CM.

In addition, we showed that RSS was able to accurately stratify the risk of CM patients with different stages (stage I, stage II, stage III, and stage IV), sex (men and women), and age (age ≥ 65 years and age < 65 years). Finally, to analyze the effects of age, sex, AJCC stage, and RSS on the prognosis of CM patients and to quantify the contribution of each index to the prognosis, we constructed the prognostic nomogram for CM patients. The results of the training and the validation cohorts showed that the prediction ability of this model was better than that of RSS or AJCC stage alone. The results of GSEA showed that the pathways related to tumorigenesis were enriched in the high-risk score group. However, the pathways that were enriched in the low-risk score group were mainly the immune response-related pathways. This further implies that the immune activity of the low-risk score group is strong, and the immunotherapeutic effect is good, while the high-risk score group has low immune activity, frequent carcinogenic mutations, and poor therapeutic effect.

Our study found that KIR2DL4 was highly expressed in CM compared with normal skin tissues, and multivariate Cox regression analysis suggested that it was an independent protective factor for the prognosis of CM patients (HR = 0.640, $p < 0.05$). In addition, the expression of KIR2DL4 was significantly decreased in the OG and the high-risk score group. Therefore, we speculated that the high expression of total KIR2DL4 in the YG and the low-risk score group increased the activity of immune cells such as NK cells and T cells, thereby enhancing the immune activity and improving the prognosis and immunotherapy effect of these CM patients. The results of immunofluorescence showed that KIR2DL4 was co-located with NK cells, and the overall prognosis and immunotherapy effect of CM patients with high expression of KIR2DL4 were better than those with low expression. In addition, the mechanism study showed that knocking down the KIR2DL4 in human NK cells in vitro can inhibit the cytotoxicity of NK cells, and can also inhibit the secretion of tumor necrosis factor-α and interferon-γ by NK cells. In contrast, upregulation of KIR2DL4 can activate the MEK/ERK signaling pathway, which is the activation pathway of NK cells.

The proproliferative transcription factor FOXM1 is the main regulator of cell cycle, which is necessary to enter the S phase and mitosis on time.[34,35] Phosphorylation of FOXM1 greatly enhances its transcriptional activity, therefore inhibiting the senescence of melanocytes.[36] In our study, as an independent risk factor for patients with CM (HR = 1.303, $p < 0.05$), FOXM1 was significantly upregulated in CM tissues compared with normal skin tissues. FOXM1 is likely to promote CM metastasis by inhibiting senescence, thereby resulting in a poor prognosis. Inactivation or loss of β_2 microglobulin (B2M) is considered to be a determinant of melanoma resistance to immune checkpoint inhibitors.[37,38] In this study, B2M was highly expressed in tumor tissues, and it was more highly expressed in the YG compared with the OG. In addition, compared with the high-risk score group, B2M was more highly expressed in the low-risk score group. The immunotherapeutic

effects of OG and high-risk score group were poorer than those of YG and low-risk score group, which is probably due to the loss and inactivation of B2M.

Both $CD8^+$ T cells and NK cells rely on cytokine IL-15 to maintain balance in vivo.[39,40] Exogenous administration of IL-15 can also promote the activation of $CD8^+$ T cells and NK cells, which has been used as an adjuvant for cancer immunotherapy.[41,42] In the present study, IL15 was more highly expressed in the YG than in the OG. In addition, compared with the high-risk score group, IL-15 was more highly expressed in the low-risk score group. Moreover, its adjuvant effect on immunosuppressive therapy may lead to better prognosis and immunotherapy effect in the YG and the low-risk score group.

In general, we developed a new RSS, which can predict the prognosis of patients with CM and the effect of immunotherapy. As the core molecule in the RSS, KIR2DL4 activated the NK cells by activating the MEK/ERK pathway, therefore promoting the release of cytotoxic factors from the NK cells and increasing the cytotoxic activity of the NK cells. Moreover, we constructed the prognostic nomogram model to better stratify the risk of CM patients and efficiently guide clinical decisions.

ACKNOWLEDGMENTS

The authors would like to thank the staff of the National Center for Biotechnology Information and the National Cancer Institute.

AUTHOR CONTRIBUTIONS

RM: Conceptualization, Experiment, Methodology, Software, Investigation, Visualization, Writing original draft. **ZR:** Experiment. **PY:** Experiment. **FY:** Experiment, Software, Investigation. **TZ:** Conceptualization, Writing – original draft, Funding acquisition, Supervision.

DISCLOSURE

The authors declare that they have no conflict of interest.

DATA AVAILABILITY STATEMENT

The data from TCGA and GEO data sets in this study are publicly available.

ETHICS STATEMENT

This study was approved by the Institutional Ethics Review Board of the Third People's Hospital of Chengdu (record #:2018S75; Chengdu, Sichuan, China), and was conducted in accordance with the Chinese ethical guidelines for human genome/gene research.

INFORMED CONSENT

N/A.

REGISTRY AND THE REGISTRATION NO. OF THE STUDY/TRIAL

N/A.

ANIMAL STUDIES

N/A.

ORCID

Rui Mao https://orcid.org/0000-0002-0135-8579
Zhengyun Ren https://orcid.org/0000-0001-5284-8976
Tongtong Zhang https://orcid.org/0000-0003-4786-5776

REFERENCES

1. Siegel RL, Miller KD, Jemal A. Cancer statistics, 2020. *CA Cancer J Clin*. 2020;70:7-30.
2. Lee S, Schmitt CA. The dynamic nature of senescence in cancer. *Nat Cell Biol*. 2019;21:94-101.
3. Fane M, Weeraratna AT. How the ageing microenvironment influences tumour progression. *Nat Rev Cancer*. 2020;20:89-106.
4. He S, Sharpless NE. Senescence in health and disease. *Cell*. 2017;169:1000-1011.
5. Leclerc J, Ballotti R, Bertolotto C. Pathways from senescence to melanoma: focus on MITF sumoylation. *Oncogene*. 2017;36:6659-6667.
6. Rajagopalan S, Bryceson YT, Kuppusamy SP, et al. Activation of NK cells by an endocytosed receptor for soluble HLA-G. *PLoS Biol*. 2006;4:e9.
7. Zheng G, Guo Z, Li W, et al. Interaction between HLA-G and NK cell receptor KIR2DL4 orchestrates HER2-positive breast cancer resistance to trastuzumab. *Signal Transduct Target Ther*. 2021;6:236.
8. Avelar RA, Ortega JG, Tacutu R, et al. A multidimensional systems biology analysis of cellular senescence in aging and disease. *Genome Biol*. 2020;21:91.
9. Subramanian A, Tamayo P, Mootha VK, et al. Gene set enrichment analysis: a knowledge-based approach for interpreting genome-wide expression profiles. *Proc Natl Acad Sci U S A*. 2005;102:15545-15550.
10. Mootha VK, Lindgren CM, Eriksson KF, et al. PGC-1alpha-responsive genes involved in oxidative phosphorylation are coordinately downregulated in human diabetes. *Nat Genet*. 2003;34:267-273.
11. Yoshihara K, Shahmoradgoli M, Martínez E, et al. Inferring tumour purity and stromal and immune cell admixture from expression data. *Nat Commun*. 2013;4:2612.
12. Aran D, Hu Z, Butte AJ. xCell: digitally portraying the tissue cellular heterogeneity landscape. *Genome Biol*. 2017;18:220.
13. Runa F, Hamalian S, Meade K, Shisgal P, Gray PC, Kelber JA. Tumor microenvironment heterogeneity: challenges and opportunities. *Curr Mol Biol Rep*. 2017;3:218-229.
14. Newman AM, Liu CL, Green MR, et al. Robust enumeration of cell subsets from tissue expression profiles. *Nat Methods*. 2015;12:453-457.
15. Becht E, Giraldo NA, Lacroix L, et al. Estimating the population abundance of tissue-infiltrating immune and stromal cell populations using gene expression. *Genome Biol*. 2016;17:218.
16. Li T, Fu J, Zeng Z, et al. TIMER2.0 for analysis of tumor-infiltrating immune cells. *Nucleic Acids Res*. 2020;48:W509-W514.
17. Shen J, Ju Z, Zhao W, et al. ARID1A deficiency promotes mutability and potentiates therapeutic antitumor immunity unleashed by immune checkpoint blockade. *Nat Med*. 2018;24:556-562.
18. Seth R, Messersmith H, Kaur V, et al. Systemic therapy for melanoma: ASCO guideline. *J Clin Oncol*. 2020;38:3947-3970.
19. Liu-Smith F, Ziogas A. Age-dependent interaction between sex and geographic ultraviolet index in melanoma risk. *J Am Acad Dermatol*. 2020;82:1102-8.e3.
20. Kaur A, Ecker BL, Douglass SM, et al. Remodeling of the collagen matrix in aging skin promotes melanoma metastasis and affects immune cell motility. *Cancer Discov*. 2019;9:64-81.
21. Byrne KT, Côté AL, Zhang P, et al. Autoimmune melanocyte destruction is required for robust $CD8^+$ memory T cell responses to mouse melanoma. *J Clin Invest*. 2011;121:1797-1809.
22. Kim SH, Cho E, Kim YI, Han C, Choi BK, Kwon BS. Adoptive immunotherapy with transient anti-CD4 treatment enhances anti-tumor

response by increasing IL-18Rαhi CD8$^+$ T cells. *Nat Commun*. 2021;12:5314.
23. Vivier E, Tomasello E, Baratin M, Walzer T, Ugolini S. Functions of natural killer cells. *Nat Immunol*. 2008;9:503-510.
24. Imai K, Matsuyama S, Miyake S, Suga K, Nakachi K. Natural cytotoxic activity of peripheral-blood lymphocytes and cancer incidence: an 11-year follow-up study of a general population. *Lancet*. 2000;356:1795-1799.
25. Coffelt SB, Kersten K, Doornebal CW, et al. IL-17-producing γδ T cells and neutrophils conspire to promote breast cancer metastasis. *Nature*. 2015;522:345-348.
26. Glodde N, Bald T, van den Boorn-Konijnenberg D, et al. Reactive neutrophil responses dependent on the receptor tyrosine kinase c-MET limit cancer immunotherapy. *Immunity*. 2017;47:789-802.e9.
27. Abbott CW, Boyle SM, Pyke RM, et al. Prediction of immunotherapy response in melanoma through combined modeling of neoantigen burden and immune-related resistance mechanisms. *Clin Cancer Res*. 2021;27:4265-4276.
28. Hodi FS, Wolchok JD, Schadendorf D, et al. TMB and inflammatory gene expression associated with clinical outcomes following immunotherapy in advanced melanoma. *Cancer. Immunol Res*. 2021;9:1202-1213.
29. Jakob JA, Bassett RL Jr, Ng CS, et al. NRAS mutation status is an independent prognostic factor in metastatic melanoma. *Cancer*. 2012;118:4014-4023.
30. Thumar J, Shahbazian D, Aziz SA, Jilaveanu LB, Kluger HM. MEK targeting in N-RAS mutated metastatic melanoma. *Mol Cancer*. 2014;13:45.
31. Randic T, Kozar I, Margue C, Utikal J, Kreis S. NRAS mutant melanoma: towards better therapies. *Cancer Treat Rev*. 2021;99:102238.
32. Robert C, Schachter J, Long GV, et al. Pembrolizumab versus ipilimumab in advanced melanoma. *N Engl J Med*. 2015;372:2521-2532.
33. Tentori L, Lacal PM, Graziani G. Challenging resistance mechanisms to therapies for metastatic melanoma. *Trends Pharmacol Sci*. 2013;34:656-666.
34. Wang X, Kiyokawa H, Dennewitz MB, Costa RH. The Forkhead box m1b transcription factor is essential for hepatocyte DNA replication and mitosis during mouse liver regeneration. *Proc Natl Acad Sci U S A*. 2002;99:16881-16886.
35. Laoukili J, Kooistra MR, Brás A, et al. FoxM1 is required for execution of the mitotic programme and chromosome stability. *Nat Cell Biol*. 2005;7:126-136.
36. Anders L, Ke N, Hydbring P, et al. A systematic screen for CDK4/6 substrates links FOXM1 phosphorylation to senescence suppression in cancer cells. *Cancer Cell*. 2011;20:620-634.
37. Restifo NP, Marincola FM, Kawakami Y, Taubenberger J, Yannelli JR, Rosenberg SA. Loss of functional beta 2-microglobulin in metastatic melanomas from five patients receiving immunotherapy. *J Natl Cancer Inst*. 1996;88:100-108.
38. Germano G, Lu S, Rospo G, et al. CD4 T cell-dependent rejection of Beta-2 microglobulin null mismatch repair-deficient tumors. *Cancer Discov*. 2021;11:1844-1859.
39. Surh CD, Sprent J. Homeostasis of naive and memory T cells. *Immunity*. 2008;29:848-862.
40. Zhou X, Yu J, Cheng X, et al. The deubiquitinase Otub1 controls the activation of CD8$^+$ T cells and NK cells by regulating IL-15-mediated priming. *Nat Immunol*. 2019;20:879-889.
41. Liu K, Catalfamo M, Li Y, Henkart PA, Weng NP. IL-15 mimics T cell receptor crosslinking in the induction of cellular proliferation, gene expression, and cytotoxicity in CD8$^+$ memory T cells. *Proc Natl Acad Sci U S A*. 2002;99:6192-6197.
42. Teague RM, Sather BD, Sacks JA, et al. Interleukin-15 rescues tolerant CD8$^+$ T cells for use in adoptive immunotherapy of established tumors. *Nat Med*. 2006;12:335-341.

SUPPORTING INFORMATION

Additional supporting information can be found online in the Supporting Information section at the end of this article.

How to cite this article: Mao R, Ren Z, Yang F, Yang P, Zhang T. Clinical significance and immune landscape of KIR2DL4 and the senescence-based signature in cutaneous melanoma. *Cancer Sci*. 2022;113:3947-3959. doi: 10.1111/cas.15499